Supporting information

Nonadiabatic molecular dynamics analysis of hybrid Dion-Jacobson 2D lead Iodide perovskites

Ying Wang† ‡, Laurent Pedesseau‖, Claudine Katan▽, Jacky Even‖, Oleg V. Prezhdo†, Sergei Tretiak‡, Dibyajyoti Ghosh‡§*#, Amanda J. Neukirch‡*
† Department of Chemistry, University of Southern California, Los Angeles, California 90089, United States
‡ Theoretical Physics and Chemistry of Materials, Los Alamos National Laboratory, Los Alamos, New Mexico 87545, United States
‖ Univ Rennes, INSA Rennes, CNRS, Institut FOTON, UMR 6082, Rennes F-35000, France
▽ Univ Rennes, ENSCR, INSA Rennes, CNRS, ISCR (Institut des Sciences Chimiques de Rennes), UMR 6226, Rennes F-35000, France
§ Center for Nonlinear Studies, Los Alamos National Laboratory, Los Alamos, New Mexico 87545, United States

Department of Materials Science and Engineering and Department of Chemistry, Indian Institute of Technology, Delhi, New Delhi 110016, India

* Corresponding Authors: dibyajnc@gmail.com; ajneukirch@lanl.gov

Computational Methods:

We used the Vienna Ab initio simulation package (VASP) for the static electronic structure calculations and AIMD simulations. The projected augmented wave (PAW[1]) method within a plane-wave basis set of cut-off energy of 400 eV are applied for all the static calculation. The generalized gradient approximation (GGA) with the Perdew−Burke−Ernzerhof functional (PBE[2]) form has been used to describe the exchange and correlation interactions. In geometry optimization, all interatomic forces of simulation cells were relaxed to less than 0.02 $eVÅ^{-1}$. Cell shapes and cell volumes are fixed, and atomic positions are allowed to change during the geometry optimization. Note that experimentally reported structures were at room temperature whereas DFT-based cell parameter optimization can only be done at 0 K. Such simulated optimized structures can modify the geometries of 2D perovskites, making these significantly different from the experimentally reported one. To avoid this discrepancy, we have kept the experimental cell parameters unchanged while performing our computational simulations. We adopted $4\times 4\times 2$ Monkhorst-Pack **k**-point mesh to sample the Brillouin zone. The DFT-D3[3] method as formulated by Grimme was included to consider vdW corrections. To get more accurate electronic structures, spin−orbit coupling (SOC) was further applied when we calculated effective masses. We used Q-Chem 5.2.1[4] to calculate the dipole moments. In this calculation, we applied 6-31G** basis set and the PBE method. More details can be found in the “dipole moment calculation method” below. Average partial (band decomposed) charge density at Γ point is calculated by summing over all the partial (band decomposed) charge density of every structure along the trajectory and then taking the average and projecting it onto the averaged structure along the trajectory.

For AIMD simulations, we had a plane-wave energy cutoff of 400 eV with a 2 × 2 × 1 Monkhorst-Pack k-point mesh, and a time step of 1fs. In these AIMD calculations, we used PBE-GGA exchange-correlation functions and DFT-D3 corrections. SOC is not included in the MD calculation. The 260 atoms unit cell prohibits its inclusion during MD. As this study is focused on comparing two systems that only differ by organic spacer cations, the effects of SOC should be comparable for both systems. We started with the 0 K DFT optimized structures and heated these structures to 300 K using repeated velocity rescaling for 2 ps and additional 1 ps trajectories using the canonical ensemble were generated to ensure thermal equilibrium. Following that, we generated 5ps trajectories in the microcanonical ensemble and then used these trajectories for the nonadiabatic coupling simulations. To investigate the charge carrier dynamics of systems, we first studied radiative recombination. The Einstein coefficient for spontaneous emission, A_{21} is adopted to calculate the radiative lifetime. We averaged over all the oscillator strength near band edges of all the structures along the 5ps AIMD trajectory and then obtained the average emission oscillator strength. Then, we apply the Einstein coefficient A_{21} and got the estimated radiative lifetimes. We used the VASP_TDM code[5] to get oscillator strength. Then we adopted PYthon eXtension for Ab Initio Dynamics (PYXAID[6-7]) code which is a mixed quantum-classical method that uses NAMD simulations to explore the nonradiative dynamics in these two systems. Since the decoherence effect is significant, we used the decoherence-induced surface hopping (DISH) technique. The number of electronic time steps per one nuclear step is 8, which is explained in “simulation details in NAMD” below. We repeat the 5 ps trajectory a couple of times to obtain a longer trajectory of 1 ns, use every 5th geometry as a starting point (1000 initial geometries in total), and calculate 500 stochastic realizations for each selected geometry to evaluate the electron-hole recombination as implemented in the PYXAID. The total sampling number is 5×10^5, which is even higher than other NAMD simulations of perovskites[8-9]. For one system, the 3AMP anti-aligned system, we used every second geometry and did not see a change in our results

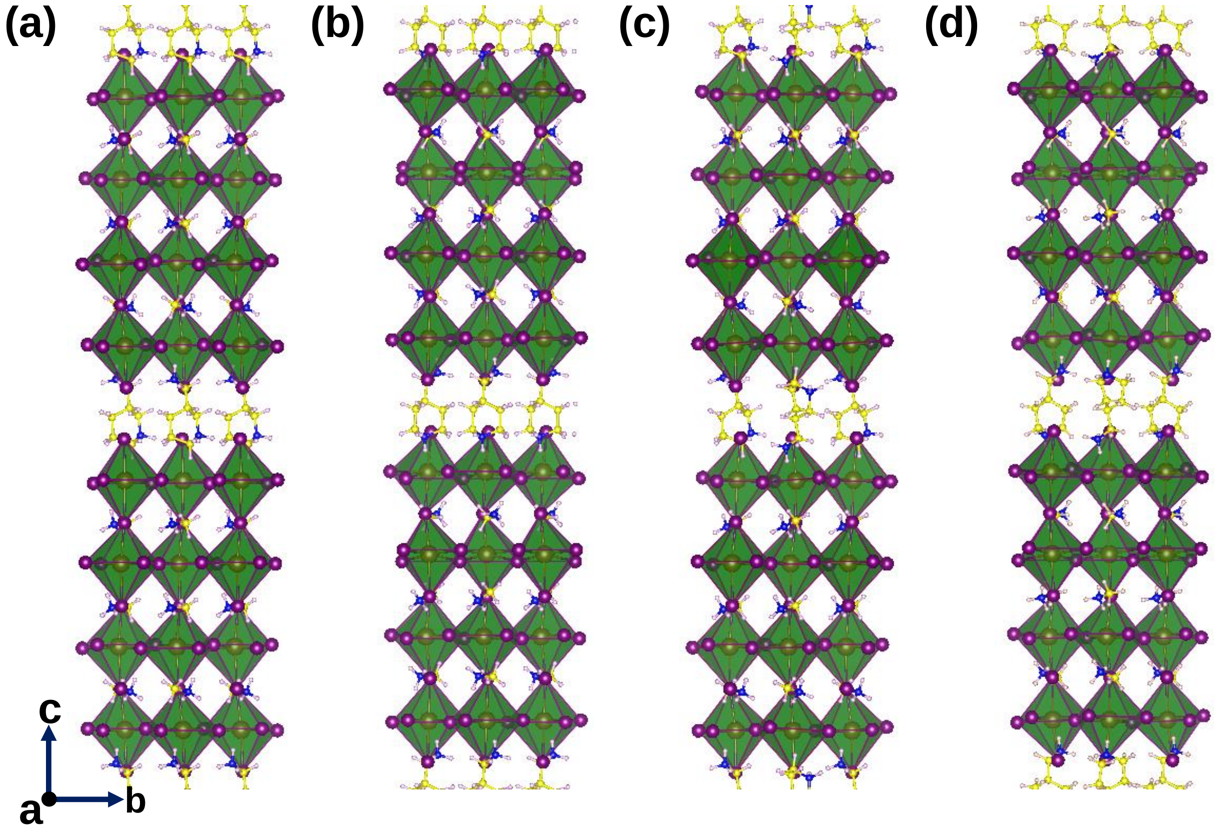

Figure S1. (a) and (b) structures of aligned **3AMP** and **4AMP.** (c) and (d) the same but for anti-aligned species. Yellow, blue, brown, purple, and pink represent C, N, Pb, I, and H atoms, respectively. The green octahedra represent the Pb-I octahedra. Axis coordination is on the left bottom.

Table S1. Total energy per simulation cell comparison between aligned and anti-aligned structures at 0 K.

species	energy (eV)	Energy difference per atom (meV)
aligned **3AMP**	-1208.907	1.16
anti-aligned **3AMP**	-1209.306	
aligned **4AMP**	-1209.208	0.81
anti-aligned **4AMP**	-1209.419	

Table S2. Calculated average Pb-I-Pb bond angle (°) and Pb-I bond length (Å) for aligned/anti-aligned **3AMP** and **4AMP**. Ax. means axial and Eq. means equatorial.

species	Ax. Pb-I-Pb bond angle	Eq. Pb-I-Pb bond angle	average Pb-I-Pb bond angle	Ax. Pb-I bond length	Eq. Pb-I bond length

aligned **3AMP**	174	152	158	3.19	3.23
anti-aligned **3AMP**	175	154	161	3.20	3.22
aligned **4AMP**	170	150	156	3.20	3.24
anti-aligned **4AMP**	166	151	155	3.21	3.24

Table S3. N-H···I bond length (Å) between inorganic layers and interlayer cations at 0K. We treat H···I as a hydrogen bond when the interatomic distance is less than 3.00 Å.

species	Average
aligned **3AMP**	2.64
anti-aligned **3AMP**	2.60
aligned **4AMP**	2.79
anti-aligned **4AMP**	2.73

Table S4. Calculated dipole moments of 3AMP/4AMP cations, aligned 3AMP/4AMP group (containing 2 aligned cations), anti-aligned 3AMP/4AMP group (containing 2 anti-aligned cations). DM refers to dipole moment. Aligned-3AMP and aligned-4AMP mean aligned-3AMP group and aligned-4AMP group, respectively. Anti-3AMP and anti-4AMP mean anti-aligned-3AMP group and anti-aligned-4AMP group, respectively. In calculation, we applied 6-31G** basis set and the PBE method.

species	3AMP	4AMP	aligned-3AMP	aligned-4AMP	anti-3AMP	anti-4AMP
DM (Debye)	4.37	3.56	9.09	6.06	1.01	4.15

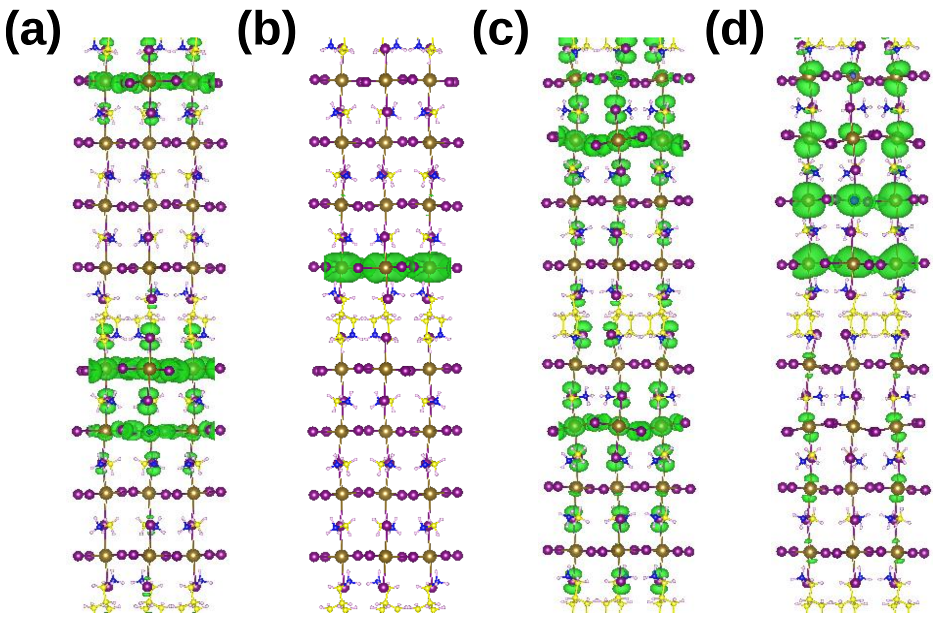

Figure S2. Partial (band decomposed) charge density at Γ point of (a) VBM and (b) CBM of aligned **3AMP** at equilibrium geometry. (c) and (d) the same but **4AMP**. SOC is not included in this partial charge density calculation.

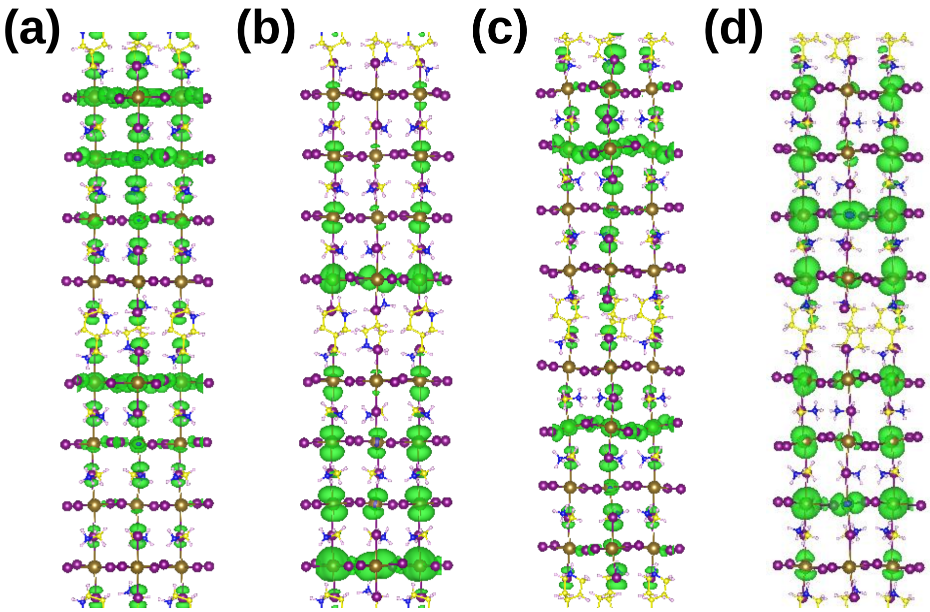

Figure S3. The same as Figure S3 but for anti-aligned species.

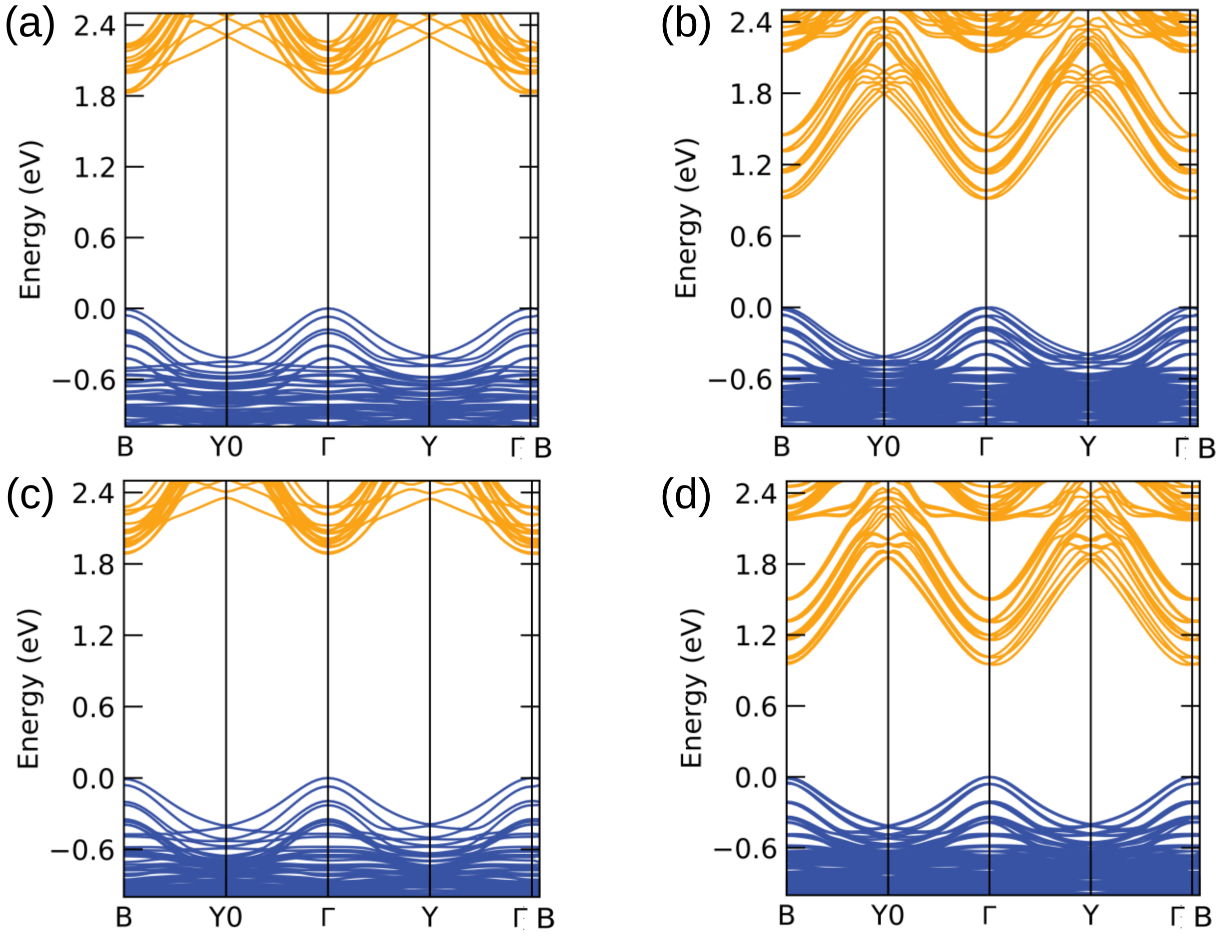

Figure S4. Band structures of anti-aligned **3AMP** (a) without SOC and (b) with SOC, anti-aligned **4AMP** (c) without SOC and (d) with SOC. In reciprocal space, the coordinate of high symmetry points: B(0.000, 0.000, 0.250), Y0(0.500, 0.000, 0.000), Γ(0.000, 0.000, 0.000), Y(0.000, 0.500, 0.000).

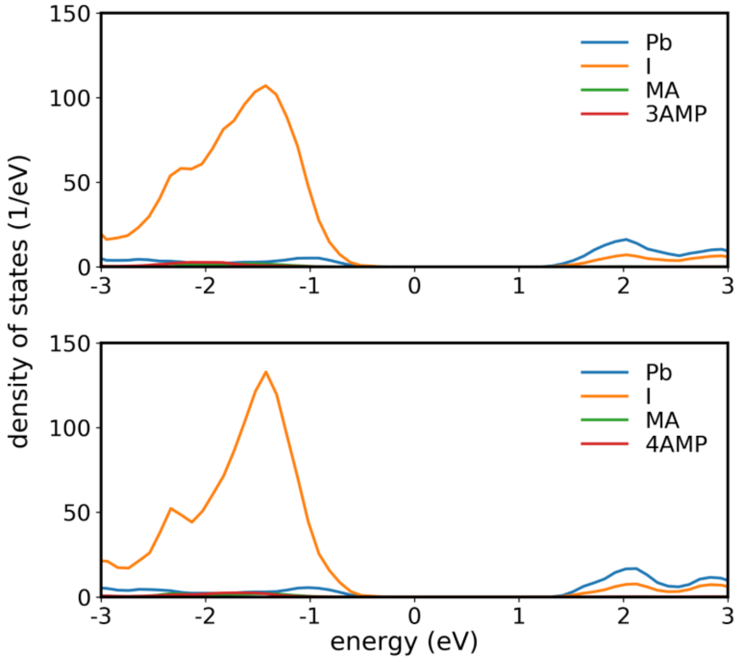

Figure S5. Projected density of states of anti-aligned **3AMP** and **4AMP** without SOC.

Table S5. Effective masses of anti-aligned **3AMP** and **4AMP**. Γ→B is along the stacking direction. B→ Y0, Γ→Y0, Γ→Y are along with in-plane directions. Some effective masses are within parenthesis because those bands are nearly doubly degenerate. The isotropic hole (m_h), electron (m_e) effective masses of $CH_3NH_3PbI_3$ reported in ref 2 and ref 3 are included for reference. All values are reported in units of electron mass (m_0). BG means bandgap (eV).

DFT-SOC	BG	direction							
		B→ Y0		Γ→Y0		Γ→Y		Γ→B	
		m_e	m_h	m_e	m_h	m_e	m_h	m_e	m_h
3AMP	0.92	0.174	-0.239	0.170	-0.386 (-0.250)	0.192	-0.267	0.632	-0.632 (-0.221)
4AMP	0.95	0.216	-0.335	0.232 (0.200)	-0.323 (-0.282)	0.213	-0.335 (-0.278)	0.630	-0.315
$CH_3NH_3PbI_3$	0.60[10]	m_e				m_h			
		0.130[11]				-0.112[11]			

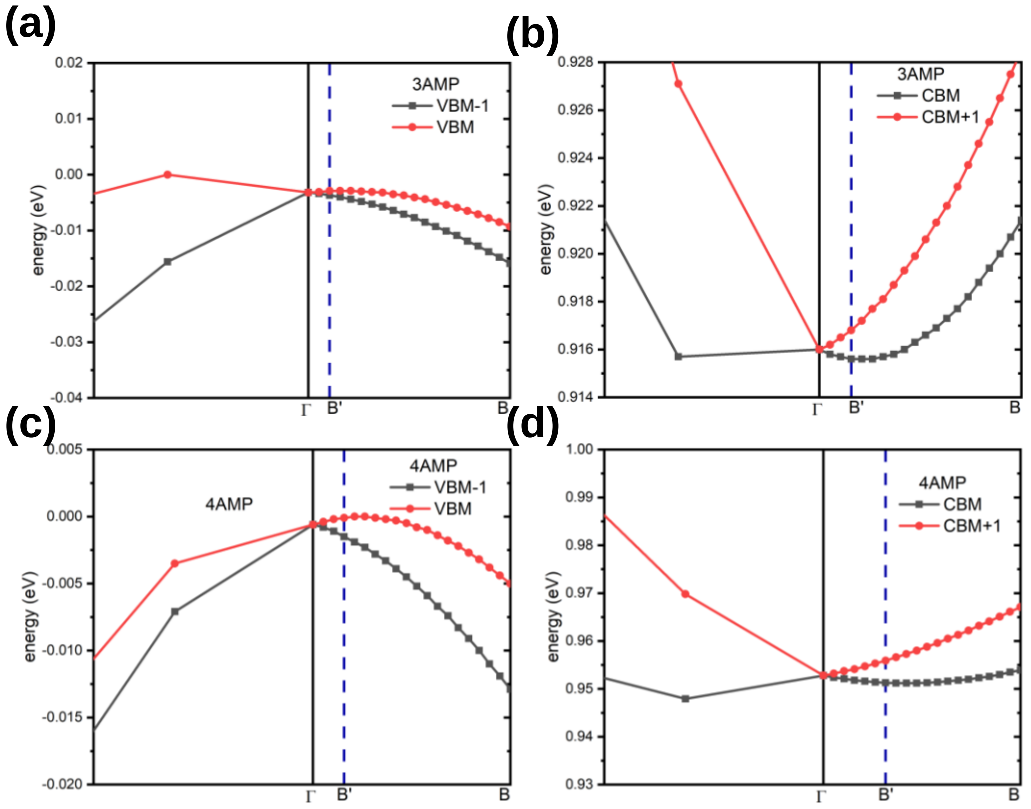

Figure S6. Close-up band distribution in reciprocal space from VBM-1 to CBM+1 of anti-aligned 3AMP and anti-aligned 4AMP when including SOC. Band distribution from VBM-1 to CBM+1 is not flat in the Γ→B region. Because of SOC, the inflection points are not exactly at Γ point and the spinors are split by a Rashba effect due to the interplay with lattice inversion symmetry breaking. We use B^' to represent the location of inflection points. (a) and (b) describe the band structure of 3AMP. (c) and (d) describe the band structure of 4AMP. For 3AMP, the inflection point of the conduction band is at CBM. While for valence band where VBM and VBM-1 are almost degenerate, VBM-1 has a greater second derivative of energy vs reciprocal path than VBM, which leads to a smaller hole effective mass derived from VBM-1 for 3AMP. For 4AMP, inflection points of the conduction band and valence band are located on CBM, and VBM, respectively. Thus, hole and electron effective masses are calculated based on the inflection points at VBM, and CBM of 4AMP, respectively.

Table S6. Averaged Pb-I-Pb bond angle (°) and I-I distance comparison, -ave means taking the time-averaged structure of the corresponding MD trajectory (300K).

species	axial	equatorial	overall	I-I distance (Å)
$CH_3NH_3PbI_3$	162.48	156.47	158.47	NA
anti-aligned **3AMP**	173.56	152.17	158.00	4.008
anti-aligned **4AMP**	169.81	150.37	155.67	4.079
anti-aligned **3AMP**-ave	172.23	165.66	167.62	4.056
anti-aligned **4AMP**-ave	173.80	155.84	161.31	4.044

Table S7. Room temperature (RT) time-averaged and equilibrium Pb-I bond length (Å) comparison.

species	axial	equatorial	Average overall Pb-I bonds
anti-aligned **3AMP** -(equilibrium)	3.193	3.231	3.218
anti-aligned **4AMP** -(equilibrium)	3.197	3.242	3.227
anti-aligned **3AMP** -(RT)	3.197	3.167	3.177
anti-aligned **4AMP** -(RT)	3.191	3.209	3.203

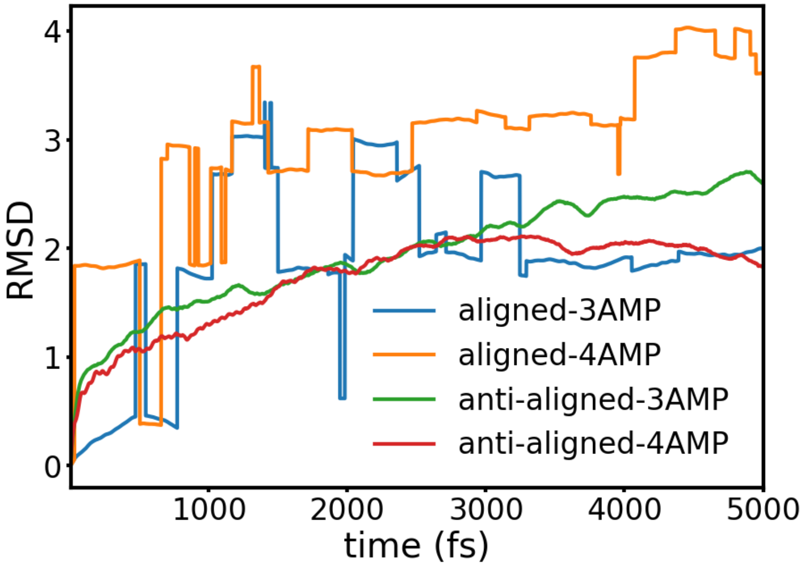

Figure S7. Root-mean-square-deviation of all atomic positions[12] of aligned and anti-aligned **3AMP** and **4AMP**.

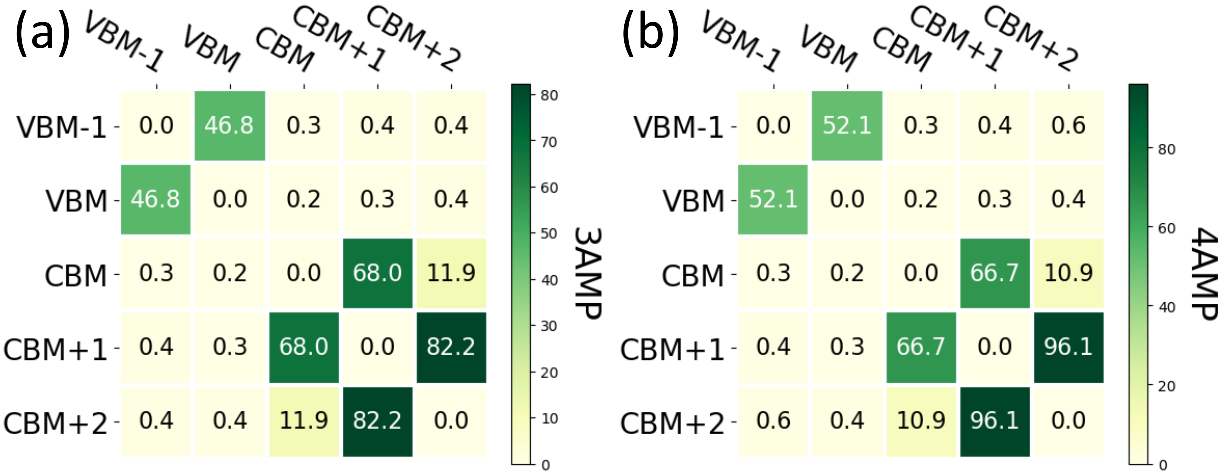

Figure S8. Nonadiabatic coupling (NAC, in meV) matrix from VBM-1 to CBM+2 of anti-aligned **3AMP** and **4AMP.**

Dipole moment calculation method[13]

The dipole moment operator is defined as:

$$\boldsymbol{\mu} = -\sum_i \boldsymbol{r}_i + \sum_A Z_A \boldsymbol{R}_A \quad \text{(S1)}$$

where $\boldsymbol{r}_i$, $\boldsymbol{R}_A$ represent electron and nuclear coordinates, respectively. Z_A is the charge of the nucleus. The x-component of the dipole moment is the expectation value of the x-component of this dipole moment operator. Y and z components of the dipole moment can be computed in the same way. Within Q-Chem the user-defined geometry gets rotated and translated into a standard nuclear orientation, where the center of the nuclear charge is always the origin.

$$<\Psi|\mu_x|\Psi> = \int [x\rho(r', r)]_{r=r'}\, dr \quad \text{(S2)}$$

Simulation details in NAMD:

In the integration of the time-dependent Schrodinger equation, there are two integration time steps, $\mathrm{d}t_{el}$ and $\mathrm{d}t_{nucl}$, corresponding to the electronic and nuclear time scales. The number of electronic time steps per nuclear step is $n_{el}=\frac{\mathrm{d}t_{nucl}}{\mathrm{d}t_{el}}$. The convergence test results of n_{el} are shown in Figure S9, it was tested up to n_{el} =10 as this was determined to be sufficient in previous works.[8] When n_{el}=8, which means $\mathrm{d}t_{nucl}$=1 fs and $\mathrm{d}t_{el}$=0.125 fs, the ground state populations converge.

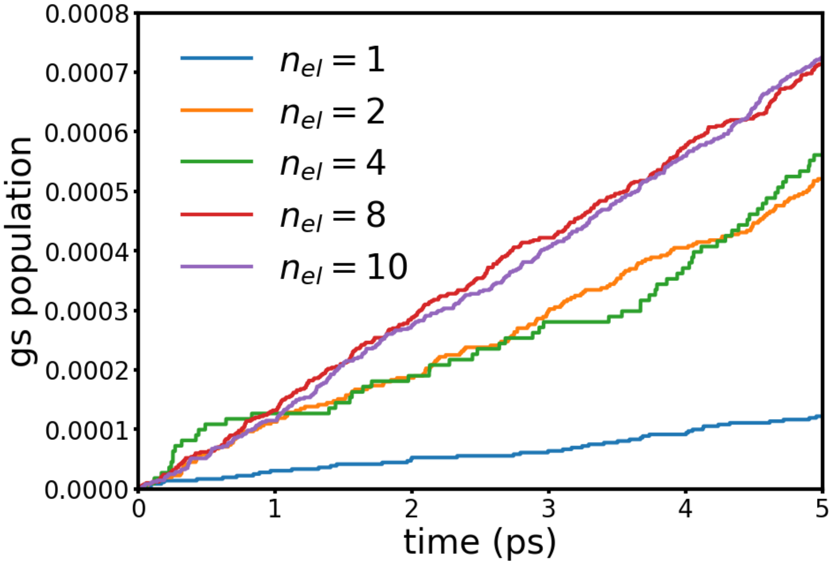

Figure S9. The convergence test of n_{el}; gs population in the y axis means the ground state population.

References:

1. Kresse, G.; Joubert, D., From ultrasoft pseudopotentials to the projector augmented-wave method. *Phys. Rev. B* **1999,** *59* (3), 1758.
2. Perdew, J. P.; Burke, K.; Ernzerhof, M., Generalized gradient approximation made simple. *Physical review letters* **1996,** *77* (18), 3865.
3. Grimme, S.; Antony, J.; Ehrlich, S.; Krieg, H., A consistent and accurate ab initio parametrization of density functional dispersion correction (DFT-D) for the 94 elements H-Pu. *The Journal of chemical physics* **2010,** *132* (15), 154104.
4. Shao, Y.; Gan, Z.; Epifanovsky, E.; Gilbert, A. T.; Wormit, M.; Kussmann, J.; Lange, A. W.; Behn, A.; Deng, J.; Feng, X., Advances in molecular quantum chemistry contained in the Q-Chem 4 program package. *Molecular Physics* **2015,** *113* (2), 184-215.
5. Qijing Zheng VASP_TDM,. https://github.com/QijingZheng/VASP_TDM.
6. Akimov, A. V.; Prezhdo, O. V., The PYXAID program for non-adiabatic molecular dynamics in condensed matter systems. *Journal of chemical theory and computation* **2013,** *9* (11), 4959-4972.
7. Akimov, A. V.; Prezhdo, O. V., Advanced capabilities of the PYXAID program: integration schemes, decoherence effects, multiexcitonic states, and field-matter interaction. *Journal of chemical theory and computation* **2014,** *10* (2), 789-804.
8. Chu, W.; Zheng, Q.; Prezhdo, O. V.; Zhao, J.; Saidi, W. A., Low-frequency lattice phonons in halide perovskites explain high defect tolerance toward electron-hole recombination. *Science advances* **2020,** *6* (7), eaaw7453.
9. Chu, W.; Saidi, W. A.; Zhao, J.; Prezhdo, O. V., Soft Lattice and Defect Covalency Rationalize Tolerance of β-CsPbI3 Perovskite Solar Cells to Native Defects. *Angewandte Chemie International Edition* **2020,** *59* (16), 6435-6441.
10. Du, M. H., Efficient carrier transport in halide perovskites: theoretical perspectives. *J. Mater. Chem. A* **2014,** *2* (24), 9091-9098.
11. Filip, M. R.; Verdi, C.; Giustino, F., GW band structures and carrier effective masses of CH3NH3PbI3 and hypothetical perovskites of the type APbI3: A= NH4, PH4, AsH4, and SbH4. *The Journal of Physical Chemistry C* **2015,** *119* (45), 25209-25219.
12. Sun, P.-P.; Bai, L.; Kripalani, D. R.; Zhou, K., A new carbon phase with direct bandgap and high carrier mobility as electron transport material for perovskite solar cells. *npj Computational Materials* **2019,** *5* (1), 1-7.
13. Krylov, A. I. Theory and Practice of Molecular electronic Structure. http://iopenshell.usc.edu/chem545/lectures2019/chem545_2019.pdf (accessed August 4).